Beam Hardening Correction for Computed Tomography Images Using a Postreconstruction Method and Equivalent Tissue Concept

Chun-Yuan Chen, Keh-Shih Chuang, Jay Wu, Horng-Ru Lin, and Meng-Ju Li

A postreconstruction method for correcting the beam-hardening artifacts in computed tomography (CT) images is proposed. This method does not require x-ray spectrum measurement. The authors assumed that a pixel in a CT image can be decomposed into equivalent tissue percentages, depending on its CT number. A scout view of the step wedges made of these equivalent tissues was performed to obtain a beam-hardening correction curve for each tissue. Projecting through the CT image from various angles generated simulated projection data and the total thickness of each tissue along the ray. The correction term was estimated using the tissue thickness traveled by the ray, and this term was then added to its corresponding projection data. A second reconstruction using the corrected projection data yielded a beam-hardening corrected image. The preliminary results show that this method reduces beam hardening artifacts by 14% for aluminum and increased the object contrast by 18% near the aluminum-water boundary. The variation in CT numbers at different locations were reduced, and the aluminum CT number also was restored.

KEY WORDS: beam hardening, computed tomography, postreconstruction, equivalent tissue

THE X-RAY BEAM used in computed tomography (CT) consists of a distribution of photons with various energies. The effective energy of the beam shifts higher as it travels through the medium because of the preferential attenuation of low energy x-rays. The CT number is directly related to the linear attenuation coefficient of the tissue, which decreases as the effective energy of x-ray increases. As a result, image reconstruction from polychromatic x-rays suffers cupping artifacts,[1] which show a decrease in CT number at the center for a uniform phantom.

The original EMI (Electro-Musical Instruments) CT scanner used a water bath[2] and was quite successful in reducing beam-hardening artifacts. However, the water bath was replaced by a wedge filter for the whole-body scanner, which revived the beam-hardening artifacts. Most CT scanners correct the projection data for beam hardening based on transmission values measured at the various water thickness'.[3,4] This correction works well for most soft tissues but fails at body areas where there is a significant amount of bone present. McDavid et al[5] used a predetermined table to convert the polyenergetic projection values into monoenergetic values. The difficulty in this method is because of the fact that a different table for each path is required.

Because of the difficulty in accessing raw projection data, Nalcioglu and Lou[6] used the postreconstruction method for beam-hardening corrections. They estimated the bone and tissue length obtained from an initial reconstruction. A correction term can be calculated from knowledge of the x-ray spectrum. A second reconstruction using these corrected projections yields a corrected image. Their method is limited to only 2 components. Furthermore, this technique requires a measurement of the x-ray spectrum, which is cumbersome to perform. Joseph[7,8] extended the postreconstruction method to any number of compounds. They used the effective density concept to establish a relationship between the CT numbers and the mass density of materials to estimate the path integrals for each material. Given this input, an equation is solved numerically to yield a correction term that can be subtracted from the reprojected data. This method also requires an estimate of the spectrum and, in addition, identification of those regions in the image that contain materials of interest.

In this research, we used a histogram of a CT image to determine the relationship between the pixel value and the equivalent tissues. Using this relationship, each pixel can be transformed into a

From the Department of Nuclear Science, National Tsing-Hua University; the Department of Radiology, National Military Kee-lung General Hospital; and the Department of Radiology, Provincial Hsinchu General Hospital, Taiwan.

Address reprint requests to Keh-Shih Chuang, PhD, Associate Professor, Department of Nuclear Science, National Tsing-Hua University, Hsinchu, Taiwan 30043.

This work is supported in part by NSC88-2212-E-007-045 provided by the National Science Council, Taiwan.

0897-1889/01/1402-0002$35.00/0

doi:10.1053/jdim.2001.24174

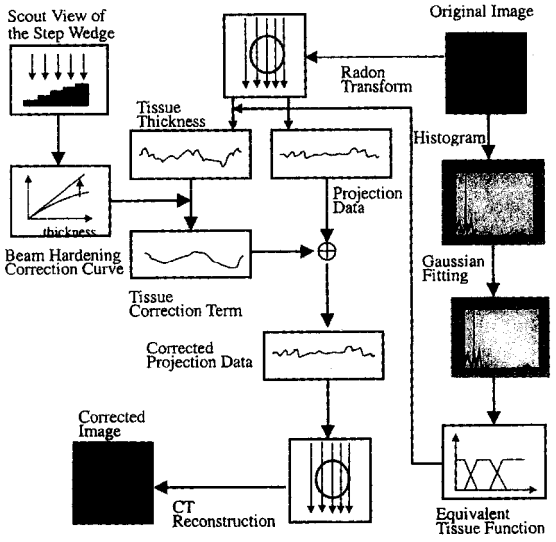

Fig 1. Flow chart of the beam-hardening correction method.

percentage for various equivalent tissues. We then used a postreconstruction method to estimate the total thickness of each equivalent tissue in the ray and perform a beam-hardening correction for each tissue. The beam-hardening correction term for each equivalent tissue was derived beforehand from a scout view of the step wedges made from the same materials. By performing this procedure, we avoid having to measure the spectrum. The advantage of this method lies in its simplicity and accuracy.

MATERIALS AND METHODS

Two phantoms were used for this study. The first phantom was a water tank (30 × 6 × 20 cm) with 2 aluminum plates (6 × 5 × 0.5 cm and 8 × 5 × 0.5 cm) inserted. The second phantom was a CT linearity performance phantom (Nuclear Associates 76-410-4130EX; Carle Place, NY). This phantom was an 8.5-inch diameter acrylic tank filled with water containing 1-inch diameter contrast pins of polyethylene (0.95 g/mL), polystyrene (1.05 g/mL), nylon (1.10 g/mL), acrylic (1.19 g/mL), and polycarbonate (1.20 g/mL). Additionally, a ¼-inch thick Teflon band was positioned at the base of the tank, concentric to the 8-inch internal diameter, to simulate human bone. The experiments were performed using a GE (Milwaukee, WI) ProSpeed Plus CT scanner. The voltage used was 120 kVp, and the slice thickness was 3 mm. A CT scanner has a soft tissue correction in the reconstruction algorithm, thus, only the beam hardening required for the aluminum was considered in this study. A simulated projection was constructed from 450 parallel beam projections encircling 180° of the CT image. A filter back-projection, using Ram-Lak filters had the highest signal-to-noise ratio in the reconstructed image and was used throughout this study.[9] To test the effect of filtering on the beam-hardening correction, we also performed a CT reconstruction using a low-pass cosine filter.[10] The diagram in Fig 1 illustrates this method.

Equivalent Tissue

We assume the reconstructed object to consist of various equivalent tissues. A histogram of the CT image was used to determine the distribution percentage for each tissue in the object.[11] Fig 2A is a histogram of a CT image. As can be seen, there are 4 peaks in the histogram representing 3 materials (aluminum, Lucite, and oil) and air. Using a Gaussian function to fit each peak, one can define a range specified by the full width at one tenth of the maximum of this function. This range represents the extent of CT numbers for that material. The ranges of different materials may or may not be overlapping.

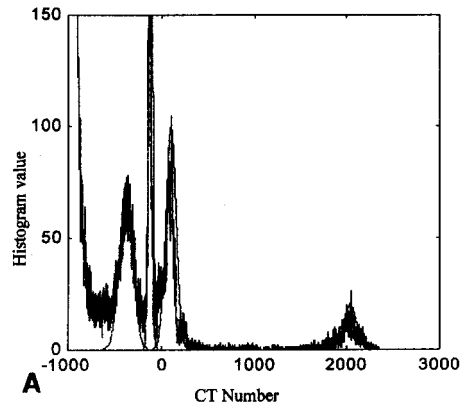

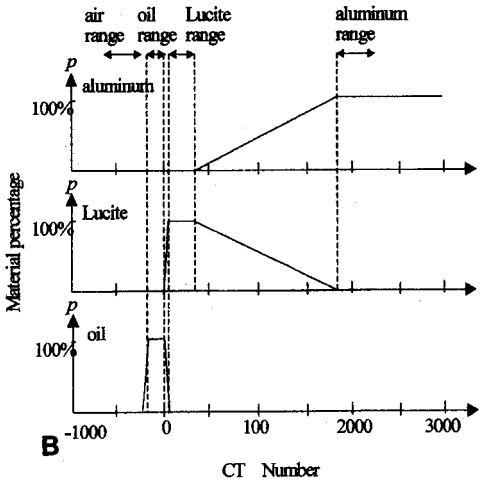

Fig 2. (A) The histogram of a CT image and the Gaussian curves fitting for the peaks with arrow indicates the range for each peak. (B) The tissue equivalent function derived from the histogram for the 3 tissues.

From these ranges, one can construct 3 (neglect air) tissue equivalent functions (Fig 2B). Each function represents the percentage of that tissue inside a pixel as a function of the CT number. In other words, any pixel can be decomposed into these 3 equivalent tissues at various percentages depending on the CT number, and the sum of these percentages is always 1. In this case, the peak location and its range for aluminum, Lucite, and oil are (2,035, 150), (100, 120), and (−120, 44), respectively. Thus, a pixel with a CT number greater than 1,885 is 100% aluminum. A pixel with a value equal to 1,050 is roughly 50% aluminum and 50% Lucite. For clinical images, the partial volume effect will generate a new pixel with its CT number is volume averaging of combined materials. This pixel can be partitioned into the equivalent tissues according to the tissue equivalent functions.

Beam-Hardening Correction Curve

A calibration phantom consisting of 3-step wedges was made of salad oil, Lucite, and aluminum (6061 alloy: Al [98%], Mg [1%], Si [0.6%]), was used to generate the beam-hardening correction curves. There are 20 steps for aluminum (0.5 cm to 11 cm with 0.5 cm increment), 20 steps for Lucite (1 cm to 20 cm with 1-cm increment), and 10 steps for oil (1 cm to 19 cm with 2-cm increment). Aluminum and Lucite were used because their atomic numbers are close to the effective atomic numbers of compact bones and soft tissues, respectively. The correction curve can be obtained from scanning the calibration phantom using the scout view technique of a CT scanner. Note, that for some scanners, the filters for scout view and axial scan may be different. For our system, both scans used the same bowtie filter. With the readings from each step wedge, one can construct a curve representing the attenuation, defined as the negative logarithm of the ratio of transmitted to incident intensities, of that material at various thickness' (Fig 3). The decrease in the slope of the attenuation curve with increasing thickness is caused by beam hardening. A straight line can be derived from the initial slope of the curve representing the attenuation of a monoenergetic beam with energy equal to the effective energy of the x-ray spectrum. The discrepancy between the straight line and attenuation curve at any thickness is the correction term for the beam hardening of that material.

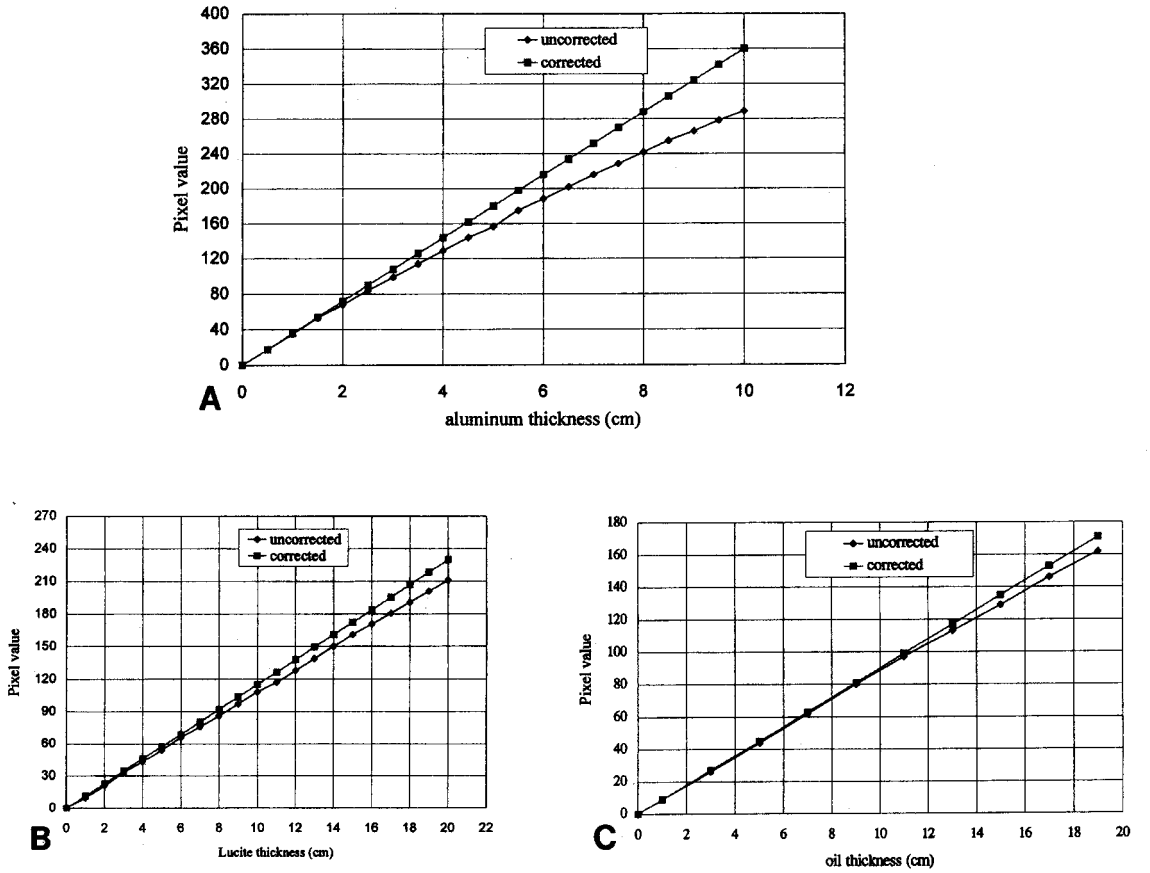

Fig 3. Beam-hardening correction curve for (A) aluminum, (B) Lucite, and (C) oil. The data were measured from the scout view images of step wedges for each tissue. The straight line is derived from taking the initial slope of the curve where the beam-hardening effect is insignificant.

Thickness of Equivalent Tissue

A Radon transform was performed to calculate the projection data as well as the total thickness for each equivalent tissue. The total tissue thickness L_i along the ray with projection angle θ and distance to center t can be calculated using the following equation:

$$L_i(t,\theta) = \sum_{x\cos\theta + y\sin\theta = t} b(x,y)p_i(f(x,y)) \quad (1)$$

where $f(x,y)$ are the CT numbers of the pixel, $b(x,y)$ is the length of the intersection of the pixel (x,y) and the ray, p_i, is the tissue equivalent function representing the percentage of tissue i in the pixel.

K Value

Note that the gray levels in the scout view image (used to generate beam hardening correction curve) and CT image (used to calculate the projection data) have different units. There is a fixed relationship between these 2 gray levels. Denote the CT number summation along the direction the beam traveled as the *CT_sum*. Define the constant *K* as the ratio between the *CT_sum* and the reading in the scout view at the appropriate position. To determine the dependence of the *K* value on the tissue thickness, we performed a scout view and several CT scans on a right cylinder phantom (Fig 4A) made of aluminum. The phantom was composed of 10 cylinders with diameters varying from 1 to 10 cm. A CT scan, with the center on the cylinder's axis, was performed for each cylinder. The *CT_sum*, passing through the center of the cylinder along the vertical line (as used by the beam in the scout view mode), was calculated for each CT image. (The *CT_sum* for rays with angles of 0, $\pi/4$, and $3/4\pi$ also were calculated. There were no significant differences observed among these rays.) The grey levels (*G_sv*) at the center of each cylinder in the scout view image were obtained. The *CT_sum*, *G_sv*, and *K* (=*CT_sum/G_sv*) values were plotted as a function of aluminum thickness in Fig 4B. The *K* value was found to be a constant (986.7 ± 19.3) independent of the aluminum thickness.

The theoretical aluminum CT value (CT_{al}) can be obtained by equating the *G_sv* and *CT_sum* for a known thickness of aluminum. From Fig 3A, the corrected *G_sv* of aluminum at a thickness of 5 cm is 180. The *CT_sum* for aluminum in the CT image with the same thickness is equal to $CT_{al} \times 5/.069$, where .069 cm is the pixel size. Thus, CT_{al} was found to be equal to 2,481 ($986.7 \times 180 \times .069/5$).

Reconstruction

Once we know the total thickness of each material in the ray, the correction term can be determined from the beam-hardening correction curve (Fig 3). The constant *K* for that material is multiplied by the correction curve value to yield the correction term (in CT number). The correction term for each equivalent tissue is then summed and added back into the projection data. Finally, these new projection data are reconstructed using a filtered back-projection algorithm to yield a corrected CT image.

RESULTS AND DISCUSSION

Figure 5 shows the original and corrected CT images of the water tank phantom. Fig 5C is the difference between Fig 5A and Fig 5B. It represents the correction performed using this method. It can be seen that the correction was performed primarily on the aluminum plate with no effect on the other materials. Figures 6A and 6B plot the horizontal profile across the original and corrected CT images, respectively. Note that the 2 peaks of the aluminum plates in the original image show different CT numbers. This is because of the heavier attenuation of the right plate. After correction, the contrast near the aluminum/water boundary in the CT image is enhanced. The contrast increases from 1711.0 (The average CT numbers near boundary for water/aluminum are 95.0 ± 61.0/1806.0 ± 120.5, respectively.) to 2005.2 (52.1 ± 63.0/2057.2 ± 188.5) for the left plate and from 1651.6 (28.8 ± 25.6/1680.4 ± 47.4) to 1948.8 (−6.6 ± 24.0/1942.2 ± 94.2) for the right plate as indicated by arrows in the combined profile (Fig 6 C). There is about an 18% increase in the contrast.

The CT numbers for water at 5 different locations (each with a 3 × 3 window) for both the original and

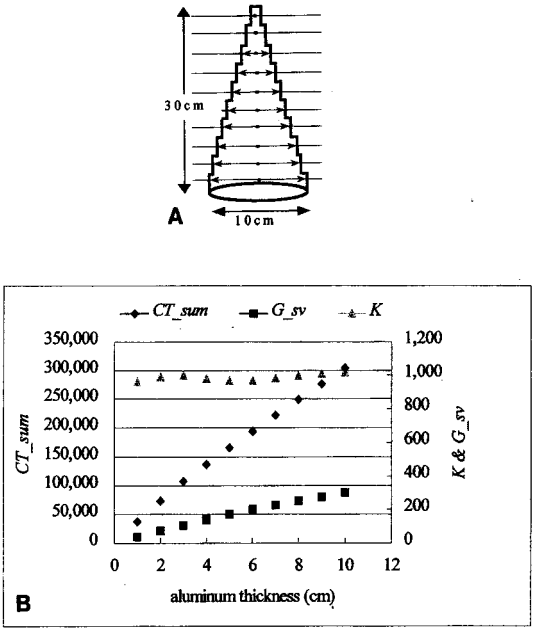

Fig 4. (A) Right cylinder phantom. Dashed lines indicate the CT scanning position. The arrows indicate the CT number (*CT_sum*) summation range calculated in the image. The pixel value (*G_sv*) is read at the dot position from the scout image. (B) The *CT_sum*, *G_sv*, and *K* value for various aluminum thickness.

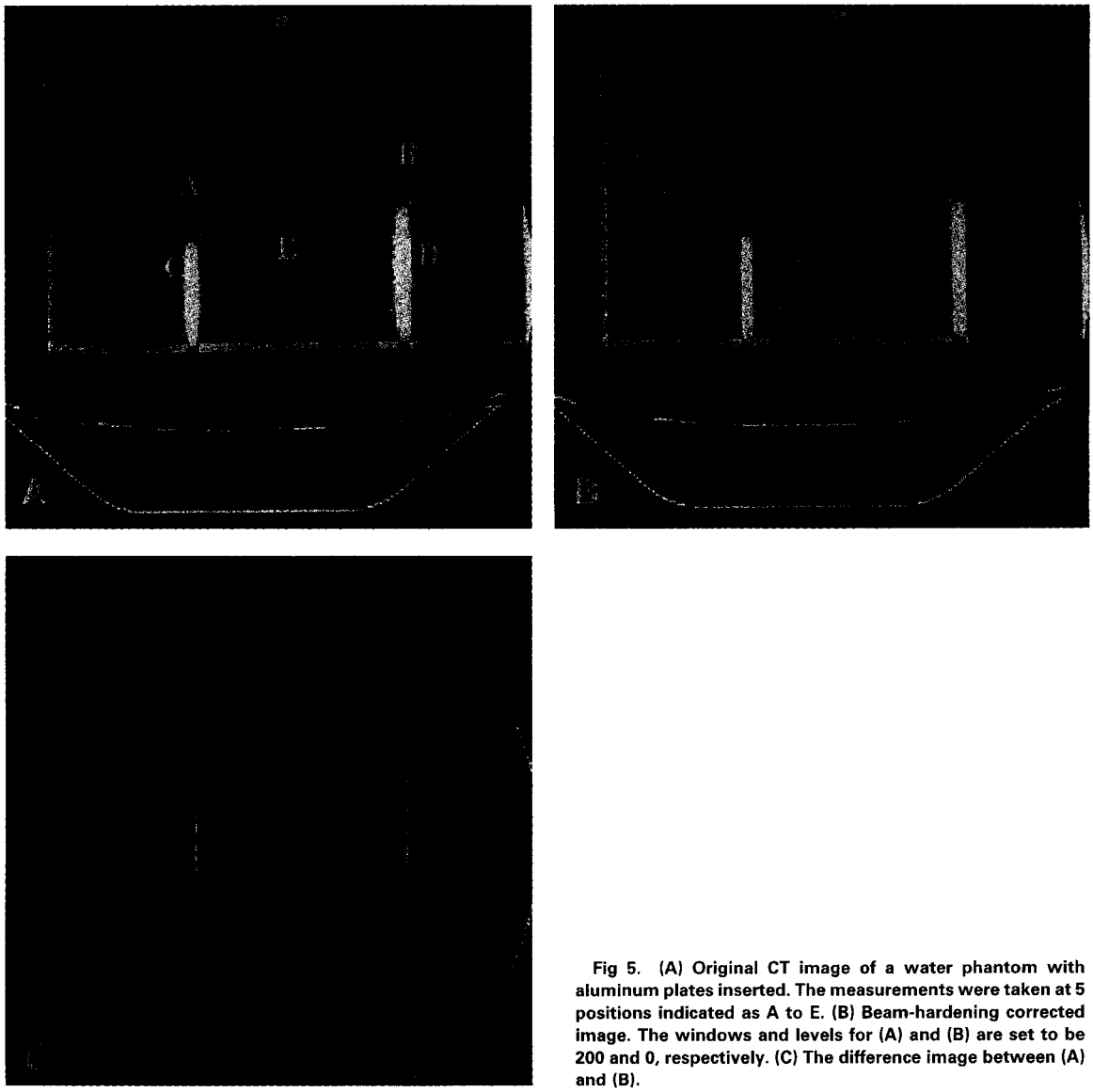

Fig 5. (A) Original CT image of a water phantom with aluminum plates inserted. The measurements were taken at 5 positions indicated as A to E. (B) Beam-hardening corrected image. The windows and levels for (A) and (B) are set to be 200 and 0, respectively. (C) The difference image between (A) and (B).

corrected images were measured, and the results are plotted in Fig 7. We can see that the variation in pixel values was most significant at locations near high-density materials (position A to D) and with almost no effect for distant locations (position E). The mean CT number for water was -14.7 ± 142.1, -8.5 ± 87.4, and -2.0 ± 91.0 for the original image and for corrected images using Ram-Lak and low-pass cosine filters, respectively. The pixel value remained nearly the same because no correction was applied to the water. The standard deviation after correction, however, shows a reduction. This was because of the correction of streak artifacts caused by aluminum using this method.

The CT numbers for aluminum were measured at 10 locations. The correction method restored the aluminum CT numbers from $1,955.6 \pm 89.4$ to $2,208.9 \pm 32.0$ for the left plate and from $1,788.2 \pm 122.8$ to $2,062.9 \pm 86.6$ for the right plate. These aluminum pixel values show an increase of about 14% in the CT number after correction.

A Linearity Performance Phantom of CT scanner with aluminum plates placed on top was scanned. The CT numbers measured at the contrast

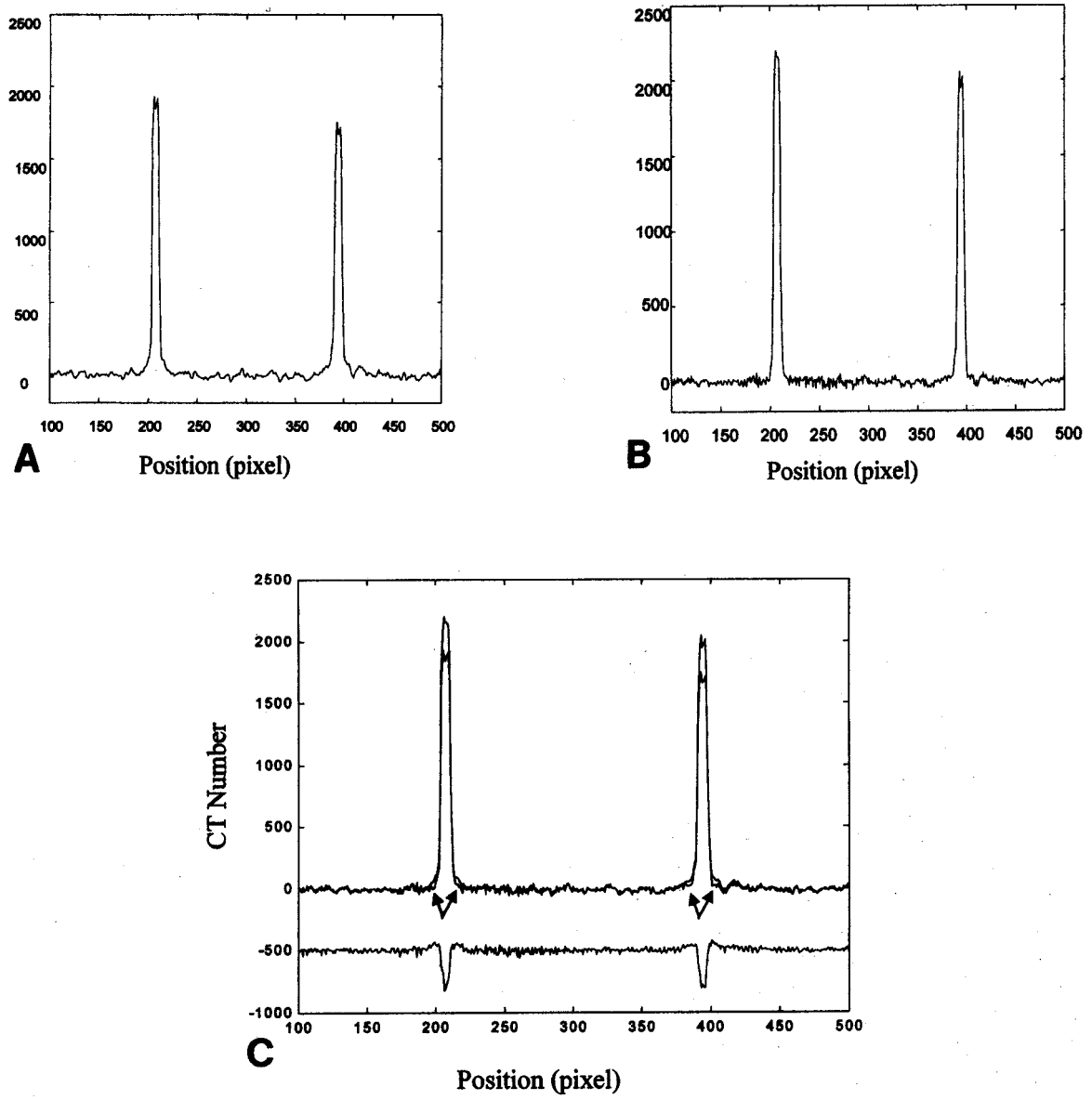

Fig 6. (A) and (B) are the gray-level profiles drawn across the original and corrected CT images. (C) plots the difference of profiles (A) and (B) and their combined profiles. The arrows indicate the shaper edges with correction. The profile difference is shifted down for better visualization.

pins and the Teflon band are summarized in Table 1. Note that there are no changes in the CT number for the materials measured. The addition of the aluminum plate causes the creation of dark streaks between the plate and the bottom of the phantom. The aluminum plate pixel value is 2,203.4 ± 22.8, which is slightly below the theoretical CT number. Because of the small size of the plates, the beam hardening effect is less severe (larger CT number) than that in the water tank (Fig 6).

There are some observations worth mentioning here. (1) This correction method has no effects on the streak artifact. The streak artifact is caused by the effects of scatter[12] and cannot be removed by this method. (2) There is no change in the CT numbers measured at the contrast pins (Table 1).

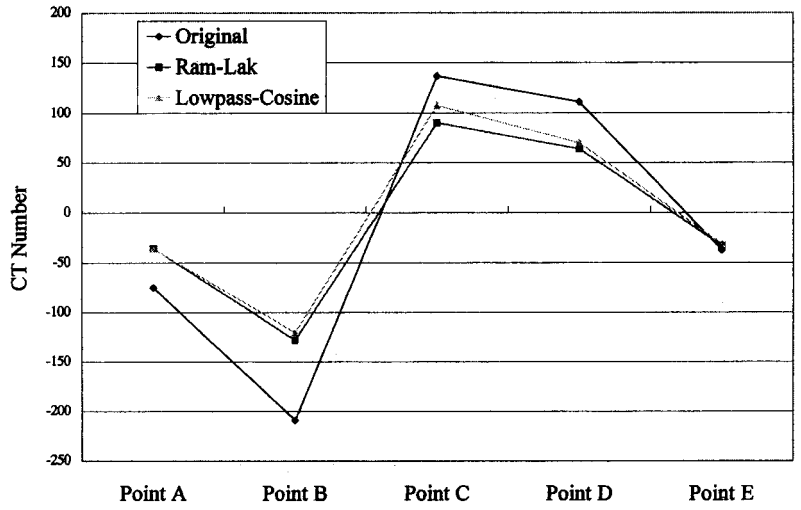

Fig 7. Pixel values of water measured at 5 locations in the original CT image, and reconstructed images using Ram-Lak and lowpass cosine filters.

(3) This correction method changes the CT number of the aluminum plate to 2,530.5 ± 41.7 (Ram-Lak) and 2,516.9 ± 38.0 (low pass cosine), which are closer to its theoretical value (2,481). The variance of the aluminum CT number is increased after correction. This is because of the projection and reconstruction procedures performed on the original CT images. (4) The CT number of Teflon was increased from 921.6 ± 18.8 to 989.5 ± 9.2 (Ram-Lak) and 981.6 ± 10.9 (low pass cosine). Because of its high CT number (921.6), the Teflon has a nonzero percentage of the aluminum. As a result, a correction term was added to Teflon.

This method is applicable to any number of materials, provided they can be distinguished in a histogram. This distinction is based on the Gaussian function fitting the distribution for each material. As long as a beam-hardening correction curve exists for the material, there is no requirement to perform a scout view of the calibration phantom.

Nasopharyngeal cancers (NPC) arise inferior to the base of the skull, and they may infiltrate into nasal fossa or infiltrate laterally and superiorly into the cranial cavity by way of the basilar foramina. Radiation treatment is the primary care for the cancer. The beam-hardening effect will reduce the accuracy of the outlining of the tumor lesion and dose calculation in treatment planning. The application of beam-hardening correction will improve the dose estimation.

CONCLUSIONS

In this report we described a method for beam-hardening correction in CT images using a postreconstruction technique and equivalent tissue concept. There is no limit to the number of equivalent tissues in the image as long as their distributions in the histogram are nonoverlapping Gaussian. The corrected image shows a reduction in beam-hardening artifacts and an increase in the object's contrast. The variations in CT numbers at different locations for both water and aluminum were reduced. The CT number for aluminum was restored to its theoretical value. The use of different filters in CT reconstruction does not significantly affect the efficiency of this method. This method does not

Table 1. CT Number Measured at Various Locations of the Linearity Performance Phantom

Material	Phantom Without Aluminum	Phantom With Aluminum	Corrected (Ram-Lak)	Corrected (Low Pass Cosine)
Polyethylene	−88.3 ± 7.9	−87.1 ± 9.1	−90.6 ± 14.4	−90.2 ± 7.5
Polystyrene	−30.0 ± 7.4	−26.4 ± 9.5	−32.3 ± 17.1	−31.9 ± 6.7
Nylon	82.7 ± 7.7	81.3 ± 9.3	80.5 ± 15.6	79.3 ± 6.4
Polycarbonate	90.1 ± 7.9	90.1 ± 8.7	84.6 ± 15.6	85.4 ± 7.3
Acrylic pin	111.8 ± 7.6	112.3 ± 8.4	107.3 ± 12.6	107.8 ± 5.8
Teflon band	917.0 ± 6.7	921.6 ± 18.8	989.5 ± 9.2	981.6 ± 10.9
Aluminum		2,203.4 ± 22.8	2,530.5 ± 41.7	2,516.9 ± 38.0

require x-ray spectrum measurements and is simple and easy to perform.

ACKNOWLEDGMENTS

The authors thank Dr Pai-Hsuen Chen of the Division of Radiation Oncology, Provincial Hsinchu General Hospital, Taiwan for his assistance in image acquisition.

REFERENCES

1. Brooks RA, Di Chiro G: Beam hardening in x-ray reconstructive tomography. Phys Med Biol 21:390-398, 1976

2. Kijewski PK, Bjarngard BE: Correction for beam hardening in computed tomography. Med Phys 5:209-214, 1978

3. Herman G: Correction for beam hardening in computed tomography. Phys Med Biol 24:81-106, 1979

4. Goodsitt M: Beam hardening errors in post-processing dual energy quantitative computed tomography. Med Phys 22:1039-1047, 1995

5. McDavid WD, Waggener RG, Payne WH, et al: Correction for spectral artifact in cross sectional reconstruction from x-rays. Med Phys 4:54-57, 1977

6. Nalcioglu O, Lou RY: Post-reconstruction method for beam hardening in computerized tomography. Phys Med Biol 24:330-340, 1979

7. Ruth C, Joseph PM: A comparison of beam-hardening artifacts in x-ray computerized tomography with gadolinium and iodine contrast agents. Med Phys 22:1977-1982, 1995

8. Joseph PM, Ruth C: A method for simultaneous correction of spectrum hardening artifacts in CT images containing both bone and iodine. Med Phys 24:1629-1634, 1997

9. Meagher JM, Mote CD, Skinner HB: CT image correction for beam hardening using simulated projection data. IEEE Trans Nucl Sci 37:1520-1524, 1990

10. Cho ZH, Jones JP, Singh M: Foundations of Medical Imaging. New York, NY, John Wiley, 1993

11. Drebin RA, Carpenter L, Hanrahan P: Volume rendering. Comput Graph 22:65-74, 1988

12. Joseph PM, Spital RD: The effects of scatter in x-ray computed tomography. Med Phys 9:464-471, 1982